Material Matters™

VOLUME 17 • NUMBER 3

Powering Tomorrow: Fuel Cells and Energy Storage

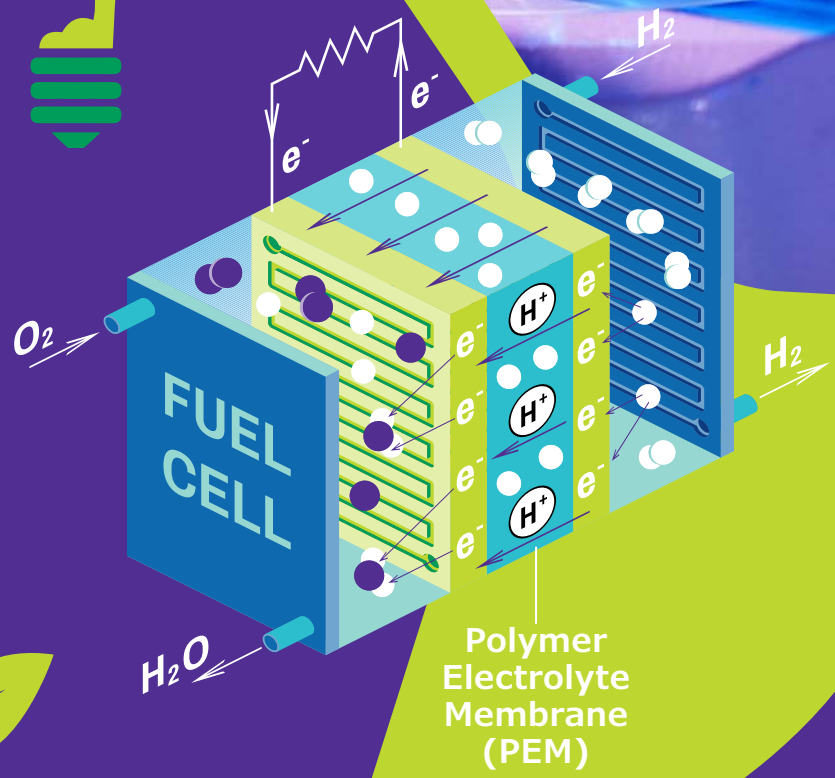

Material Matters™
VOL. 17 • NO. 3

Introduction

Megan Muroski, Ph.D.
Global Product Manager – Nanomaterials and Energy

Welcome to the final issue of *Material Matters* for 2022, focused on novel materials and innovative platforms for renewable energy. Due to the growing need for energy, technologies that can convert electricity from a renewable source into a chemical fuel for storage (and vice versa) are increasingly vital. While there are many challenges facing the widespread use of renewable energy, among the most critical are cost-effective, sustainable energy storage and conversion systems. Unlike fossil fuels, renewables don't generate electricity on demand. Although batteries have long been considered one of the most effective energy storage methods, the environmental impacts of large-scale battery use remain a significant challenge requiring inventive solutions. As technology progresses, the future development of renewable systems depends on energy storage.

In the first article, **Professor Moth-Poulson (ICREA, Spain)** looks at Molecular Solar Thermal Energy Storage (MOST) Systems, also known as solar thermal fuels (STF), as a promising approach for solar energy harvesting and storage. MOST systems play a crucial role in current renewable energy research by combining sunlight's power with molecular materials' ability to store energy. This article highlights the advantages of some of these candidates by detailing their synthesis and demonstrating how each can be tuned to increase their efficiency.

In the second article, **Professor Neto (Cidade Universitária, Brazil)** presents their perspective on fuel cell material development with a focus on ethanol and glycerol for direct alcohol fuel cells. Enormous advances have been made for the utilization of glycerol in catalytic processes, and it currently offers great potential for renewable energy generation. Additionally, the author discusses anion exchange membrane developments and challenges.

In the final article, **Professor Stimming (Newcastle University, United Kingdom)** discusses his novel innovations using polyoxometalates (POM) ions with multiple redox centers. These compounds can be applied to a modified redox flow battery concept which uses two liquids for electrodes in an electrochemical cell. POM-based battery systems have many advantages for electricity storage including capacity, power, ease of operation and transport, durability, sustainability, and eventually, low costs.

Each article is accompanied by a curated list of related products available from Merck. For more information and additional product offerings, please visit us at SigmaAldrich.com/matsci. Do you have any new product suggestions or new ideas for future *Material Matters*™ Please contact us at **SigmaAldrich.com/technicalservice**.

About the Cover

The demand for energy is increasing at an unprecedented rate. At the same time, the need to transition to sustainable and clean energy sources is more urgent than ever before. This issue highlights some exciting research technologies proposed to solve the challenges of powering the future sustainably, including solar energy storage, fuel cells, and flow batteries. An image of a fuel cell is displayed in the top right corner. A schematic representation of a fuel cell converting hydrogen and oxygen gas into electricity and water is shown in the middle. Our Material Science team is dedicated to advancing energy technologies with a comprehensive portfolio of innovative materials to empower breakthroughs.

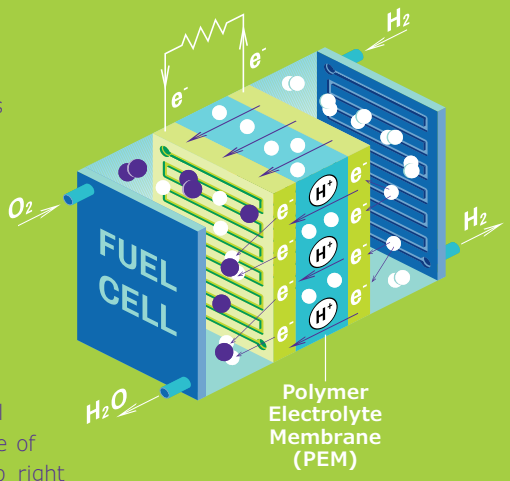

Merck KGaA
Frankfurter Strasse 250
64293 Darmstadt, Germany
Phone +49 6151 72 0

To Place Orders / Customer Service
Contact your local office or visit
SigmaAldrich.com/order

Technical Service
Contact your local office or visit
SigmaAldrich.com/techinfo

General Correspondence
Contact your local office or visit
SigmaAldrich.com/techinfo

Subscriptions
Request your FREE subscription to *Material Matters*™ at **SigmaAldrich.com/mm**

The entire *Material Matters*™ archive is available at **SigmaAldrich.com/mm**

Material Matters™(ISSN 1933-9631) is a publication of Merck KGaA and/or its affiliates

Table of Contents

Articles

Featured Products

Your Material Matters

Nicolynn Davis, Ph.D.
Head of Material Sciences and F&F

Lead sulfide-based quantum dots can absorb and emit light across the near-infrared (NIR) and short-wave infrared (SWIR) wavelengths in the electromagnetic spectrum. Quantum dot technology has been intensively researched and developed for commercial application in photodetectors, photovoltaics, and infrared light emitters.

The semiconductor band gap of lead-sulfide (PbS) quantum dots can be controlled by the particle size, whereby longer wavelength absorbing materials denote larger nanoparticles. The excitonic absorption peak wavelength can ascertain the characteristics of the quantum dot and is observed as a strongly absorbing peak at a slightly higher energy than the absorption onset. Defined as the full width at half maximum (FWHM), a narrow peak indicates a monodisperse ensemble of nanoparticles. This is highly desirable in applications where a flat energy landscape, a narrow energy distribution, and the formation of superlattices yield improved performance.

Alongside superior optical performance through synthesis, Quantum Science Ltd. surface science has developed robust materials that can withstand prolonged exposure to high temperatures. This serves as a strong indicator that the materials are resistant to shorter periods of elevated temperatures during post-processing in device fabrication.

Some potential applications of infrared PbS quantum dots include:

1. Infrared photodetectors based on solution processing of PbS nanoparticles that have reported photon conversion efficiencies of over 80%, giving excellent sensitivity in short-wave infrared (SWIR).[1]
2. Photovoltaics using PbS quantum dots that can exploit the infrared spectrum not easily accessible using traditional solar cells. This is advantageous as half of the solar energy reaching the earth is in the infrared region. These devices can be designed as single-junction solar cells or multijunction "tandem" cells.[2]
3. Infrared light-emitting diodes (LEDs) that find application in several areas, such as surveillance and security, night vision, biomedical imaging, and spectroscopy.[3]

References

(1) Vafaie, M.; et al. *Matter* **2021** *4* (3), 1042–1053. DOI:10.1016/j.matt.2020.12.017
(2) Choi, M. J.; et al. *Nat. Commun.*, **2020**, *11* (1), 1–9. DOI:10.1038/s41467-019-13437-2
(3) Pradhan, S. et al. *Nat. Nanotechnol.* **2019**, *14* (1), 72–79. DOI:10.1038/s41565-018-0312-y

Name	Cat. No.
Infrared PbS quantum dots, λ_{max} 1550 nm, 100 mg/ml in toluene	**925535**
Infrared PbS quantum dots, λ_{max} 1350 nm, 100 mg/ml in toluene	**925543**

Molecular Solar Thermal Energy Storage Systems (MOST) – Design, Synthesis, and Application


Helen Hölzel[1] and Kasper Moth-Poulsen[1,2,3*]

[1] Department of Chemistry and Chemical Engineering, Chalmers University of Technology, Kemigården 4, 412 96 Gothenburg, Sweden
[2] The Institute of Materials Science of Barcelona, ICMAB-CSIC, 08193, Bellaterra, Barcelona, Spain
[3] Catalan Institution for Research & Advanced Studies, ICREA, Pg. Lluis Companys 23, Barcelona, Spain
*E-mail: kasper.moth-poulsen@chalmers.se

Introduction

With worldwide population growth, the global energy demand has drastically increased and will rise by an average of 1.3% annually until 2040.[1] Currently, this challenge is not merely addressed by conventional energy sources such as oil, coal, gas, or nuclear power, but also by renewable energy sources such as wind and solar energy. The demand for renewable energy sources has been increasing even during the economic crisis due to lockdowns caused by the global pandemic, Covid-19.[2,3] The renewable energy share, among the total energy mix, increased to 5.7% in 2020 outnumbering nuclear energy at 4.3%.[3] The growth for wind and solar energy was 238 GW in 2020, which is 50% more than any single year in history. The sun, being most abundant among renewable energy sources, delivers around 235 Wm^{-2} on average.[4] Typically, energy from the sun is used directly for heating or electric power production; however, as renewable energy continues to grow as part of the energy mix, efficient energy storage becomes a growing challenge. A promising approach for solar energy harvesting and storage is the concept of molecular solar thermal energy storage (MOST) systems also known as solar thermal fuels (STF). Solar energy is used to drive the chemical reaction of a molecule, usually referred to as a molecular photoswitch, leading to an energy-rich metastable isomer, which stores the energy. The energy can later be released on demand, controlled thermally, catalytically, or through irradiation with selected wavelengths of light. In this article, we introduce the requirements for a MOST system, the structures of different photoswitches, their general charging and discharging mechanisms, highlight the accessibility of the material by synthetic production, and describe possible uses of the stored energy.

Molecular Solar Thermal Energy Storage (MOST) Systems

In general, MOST systems should feature at least four functional principles as illustrated in **Figure 1A**. A MOST system is based on a photochemical reaction such as isomerization, dimerization, or rearrangements. During the photochemical reaction, photon energy is converted to chemical energy by converting the parent molecule, **A** to a high-energy meta-stable photoisomer, **B** (**Figure 1**). **B** should have a high-energy storage density compared to **A**, and depending on the application, should feature a suitable storage half-life ($t_{1/2}$). The back-reaction process should result in a release of energy as heat and can be activated by either thermal activation, a catalytic system (catalyst or electrochemistry), or light. The last but most important principle is the stability and availability of the system. This includes a simple way

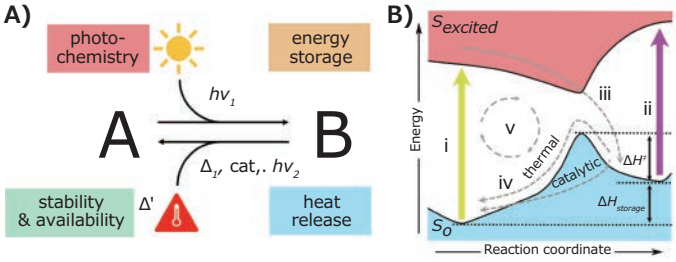

Figure 1. **A**) Schematic depiction of features of a MOST system and **B**) the MOST operation cycle, i) absorption from parent molecule to an excited state, ii) absorption from the meta-stable state, iii) photoconversion, iv) thermal or catalytic back-conversion, v) cyclability. Reproduced from reference 5, copyright 2022 Elsevier B.V.

of molecule preparation, which requires economic feasibility regarding applications. Further, the molecule should be stable for longer periods, and withstand several cycles of operation. To meet all these principles, molecular design is the most crucial point.

Before design and synthesis come into play, it is necessary to understand the energy landscape and steps of the energy storage process in more detail, to extract the most ideal concept fitting the requirements to create efficient systems.[5–7] The process consists of four main steps and a few side processes (**Figure 1B**). Exposure to light should excite molecule **A** from its ground state (S0) to its excited state (Sexcited) via photon absorption (i). To use the photons provided from solar irradiation, the system should absorb light between 300–800 nm,[8] as 50% of the incoming photons are within this range.5 Through photoconversion (iii) the excited molecule ends up in a meta-stable high energy photoisomer **B**. This process strongly depends on the photoisomerization quantum yield Φ_{iso}. Preferably, the photoisomerization should happen via one photon with a quantum yield close to 1. The molecule should then remain in this state, for longer periods indicated by the half-life time ($t_{1/2}$). Depending on the application, $t_{1/2}$ should be long enough to store the energy for days, months, or years at room temperature.[8] However, $t_{1/2}$ depends on the rate of the back-reaction (iv) and is thus intimately related to the thermal back-reaction barrier $\Delta H^{\ddagger}$. As the meta-stable isomer should store energy, the $\Delta H_{storage}$, which is the energy difference between the two isomers, should be as high as possible. To release the energy, the back-conversion (iv) can be triggered either catalytically, thermally, electrochemically, or for some compounds also photochemically. Especially the latter trigger might display a competing absorption process (ii) and should be avoided or suppressed. In the best case, the spectral overlap should be small. The trigger should be as efficient as possible to release the energy when required. Considering this is a circular process, the final, important factor is the cyclability (v) of charging and discharging of the MOST material. Within this cycle, there should be no degradation (or less degradation) and no material fatigue should be observed. Real-life applications should apply sustainability practices, meaning the material should be harmless for the environment and humans. These requirements are very specific and difficult to address in a single molecular system, creating a challenge to find the "ideal system" to apply in real-life applications. Nevertheless, the search steadily reveals important molecular features and progress in performance in all aspects previously mentioned. In the following sections, we will introduce different molecular systems that are being studied and how molecular design has been used to improve their function.

Photoswitches as MOST Materials

Through the years several different molecular systems have been investigated and suggested as MOST candidates.[5,6] Three main molecular systems are gaining increasing interest: the norbornadiene/quadricyclane (NBD/QC), the *E/Z*-azobenzene (*E/Z*-AZO), and the dihydroazulene/vinylheptafulvene (DHA/VHF) isomers (**Figure 2**).

A) Norbornadiene (NBD)/ Quadricyclane (QC)

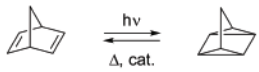

B) *E-IZ*-Azobenzene

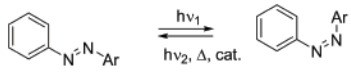

C) Dihydroazulene (DHA)/ Vinylheptafulvene (VHF)

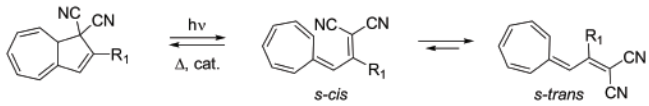

Figure 2. Examples of currently investigated MOST systems and conversion processes. **A**) norbornadiene NBD/ quadricyclane QC couple, **B**) *E-/Z*-azobenzene couple, **C**) dihydroazulene DHA/ vinylheptafulvene VHF couple.

However, while the overall goals for the use of those systems as MOST are similar, there are some differences in the charging and discharging mechanisms as well as molecular design principles for each compound class. For the NBD/QC system the molecule is excited through either direct irradiation or via the use of a photosensitizer. The chemical reaction that occurs after excitation is a [2+2] cycloaddition (**Figure 2A**). Unsubstituted NBD itself only absorbs in the UV region, therefore different design strategies have been used to optimize the system for solar absorption.[9] The quadricyclane molecule has a high internal strain and can store around 0.1 MJ mol^{-1}.[10] For some optimized compounds storage energy densities of up to 1 MJ kg^{-1} are reported.[7,11] The azobenzene system can be switched from its *E/trans*-isomer to its *Z/cis*-isomer via irradiation at the respective wavelength (**Figure 2B**).[6] However, the amount of stored energy of the parent *Z*-azobenzene (0.041 MJ mol^{-1}) is around half the value of QC,[12] and full conversion is challenging to achieve due to the photochemical equilibrium. The *Z*-isomer converts back to the *E*-isomer via light irradiation in the visible range. This competition can be mitigated using a bandpass filter for device applications[13] or by molecular engineering.[14] The DHA molecule can be converted to VHF through a photoinduced ring-opening reaction. Initially, the s-*cis* form is formed which then changes into the more stable s-*trans* conformer (**Figure 2C**).[15] The VHF usually possesses red-shifted absorption compared to DHA, similar to azobenzene, but is photochemically inactive, and thus no competing back-conversion of the visible spectral range occurs. To date, most parent molecules cannot store energy efficiently; therefore, structural, and molecular design strategies are employed to modify and optimize the properties.

Molecular Design Strategies

Addition of substituents to red-shift the absorption profile of the parent molecule A is an important objective for storage of a large fraction of the solar energy spectrum. Herein, we exemplify some strategies for the NBD molecule.[9] Attaching corresponding functionalities and substituents to the parent

molecules using a donor-acceptor pair, lowers the HOMO-LUMO gap of the system. Hereby two design approaches can be used. One approach is the introduction of donor and acceptor groups at the two different double bonds of the NBD system (**Figure 3A**).[16] These types of push-pull systems, **NBD 1**, rely on the principle of homoconjugation which promotes communication and charge transfer through space. However, this may be accompanied by an increase in molecular weight which reduces the energy storage density. Another approach is a push-pull architecture on one double bond of the molecule (**Figure 3B**, for example, **NBD 2**).[11] This results in a better match with the solar spectrum via bathochromic shifting of the absorption profile but may lead to reduced energy storage time $t_{1/2}$.

Dimeric donor-acceptor type systems, **NBD 3**, can lead to even further red-shifting of the absorption band and provide enhanced charge transfer through the bridge (**Figure 3C**).[17] Accompanied by the general design of multi-photoisomeric architectures, which feature two or more photoswitchable units. Each moiety can exhibit different thermal back-conversion barriers and thus lead to several switching events in one molecule so that the overall energy storage density increases even though the molecular weight also increases.[18] Therefore, one of the most promising approaches to date, utilizes two concepts: the extension of the conjugation within the system and the introduction of electron-donating and electron-accepting groups. Aryl and acetylene units attached to the molecular core typically led to a better match with the solar spectrum and show enhanced p-conjugation. However, this increases the molecular weight drastically, especially in the case of aryl units.[19] To counter this, one of the substituents can be replaced by a low molecular weight functionality with electron-withdrawing properties.[20] This could result in very promising candidates such as **NBD 4** (**Figure 3D**) which not only lead to bathochromic shifting of the absorption but also a higher energy density, as well as improved and persistent stability, withstanding many cycles of charging and discharging.[21] Unfortunately, in this case, a lowered $t_{1/2}$ was observed.[20] Extension of storage times for NBDs was observed by the addition of bulky substituents to the carbon bridge or the introduction of *ortho*-aryl substituents (compare **NBD 5** and **NBD 6**, **Figure 3E**). Both approaches lead to steric repulsion effects directly impacting the back-reaction barrier.[11,22]

Similar Design strategies are applied for other MOST systems, e.g. azobenzenes and DHA (**Figures 4A** and **4C**). In a recent study, substituents on the azobenzene units had stark effects on their properties (storage times, absorption profiles, isomerization quantum yield, etc.), e.g. donor-acceptor motifs or introduction of *ortho*-substituents, especially fluorinated azobenzenes (**Figure 4A** and **4B**).[6] Leading to exceptional extended half-life times caused by less electron density in the azo-bridge, thus stabilizing the *Z*-form.[6] Further half-life and red-shifting of absorption can be influenced by introducing various amino-functionalities with different p-donation properties; hence stronger donors lead to more visible range spectral overlap while weaker donors ensure longer storage times (**Figure 4B**).[23] Replacement of the phenyl-substituents in azobenzenes by using heteroaryls (**Figure 4B**), such as triazoles and pyrazoles have an impressive effect on the

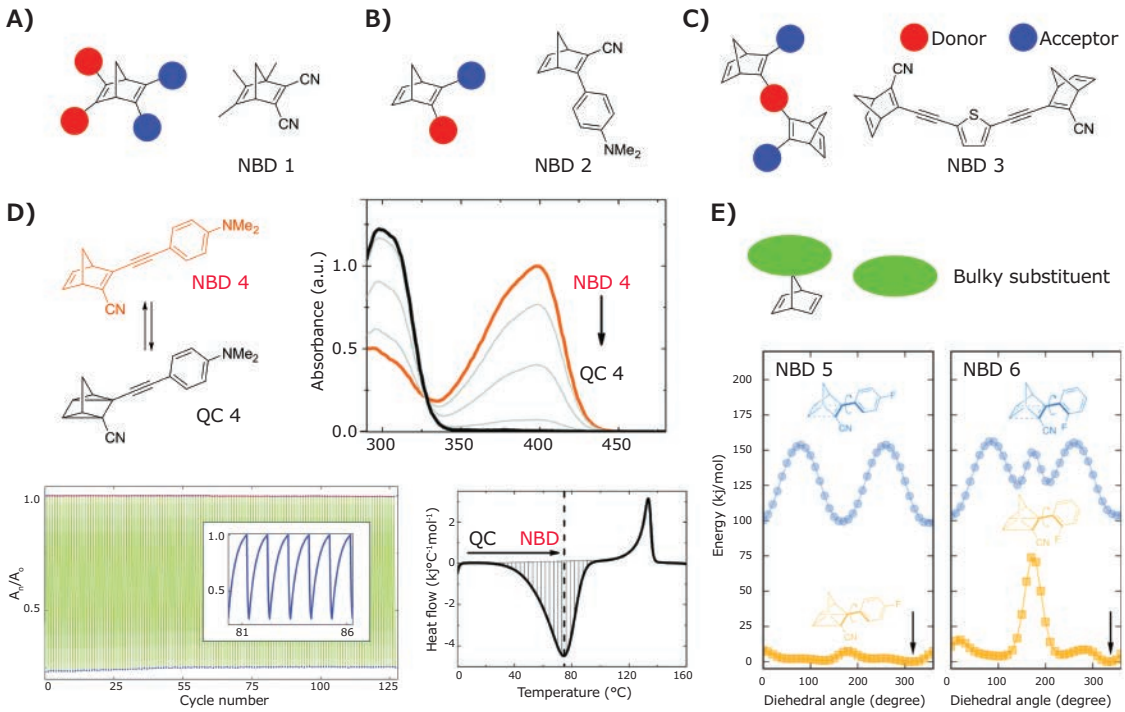

Figure 3. A–C) Different NBD donor-acceptor motifs with examples, D) example for a low-molecular weight NBD with red-shifted absorption and full conversion, high cyclability, and good heat release, E) strategy to improve half-life by introduction of bulky substituents or change in the dihedral angle using *ortho*-substituents. Figures reproduced from references 11, 20 and 21, copyright 2016 Wiley-VCH Verlag GmbH&Co. KGaA, 2018 Wiley-VCH Verlag GmbH&Co. KGaA, and The Royal Society of Chemistry 2017.

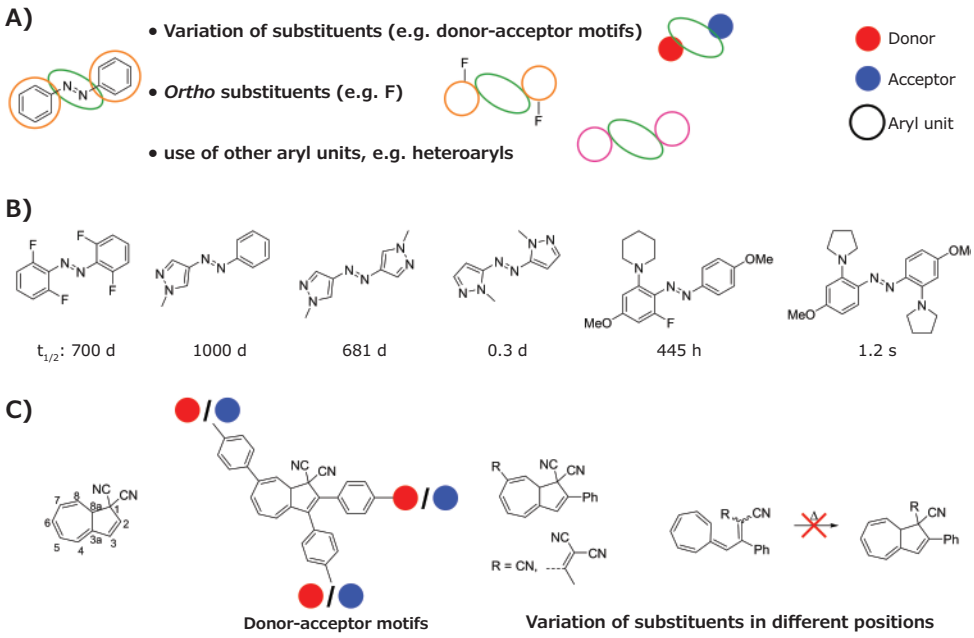

Figure 4. A) Examples for variation of azobenzene, B) concrete examples and influence on the half-life, C) numbered DHA molecule and examples for variation.

conversion, revealing complete conversion from *Z* to *E* in most of the cases.[6,14,24] In the case of bis-pyrazole systems, less steric hindrance within the molecule and the position of substitution of the heteroaryl moiety, effects the thermal back-reaction and thus the half-life of the system, due to different stabilization via intramolecular interactions.[14] Azobenzenes have also been investigated as phase-change materials for MOST applications.[25] DHA molecules are also influenced by substituents (**Figure 4C**), especially with the introduction of donor-acceptor units at the C2, C3, or C7 positions, for example, with functionalities attached to phenyl groups.[15,26,27] Hereby, longer half-lives and red-shifting of absorption were achieved, especially when using cyano-based substituents at C7.[28] Variations from one cyano group at C1 using a hydrogen atom or methyl group influence the back-reactions barrier,[29] while computations reveal that annellation of a benzene unit at the C2–C3 will increase the energy density.[30]

Synthesis and Preparation

The preparation of MOST materials is strongly dependent on the molecular system and the accompanying structural composition. In the case of NBDs, synthesis occurs primarily using two approaches: palladium-catalyzed cross-coupling reactions, or Diels-Alder reactions (**Figure 5**). The first synthesis pathway starts from the commercially available 2,5-norbornadiene (**Cat. No. 8.20918**) **1** (Bicyclo[2.2.1]hepta-2,5-diene, **Cat. No. B33803**) which reacts with brominating agents, like 1,2-dibromoethane **2**, (**Cat. No. 240656**),[31,32] or by using a lithiation followed by quenching with electrophiles, such as *p*-toluenesulfonyl halide, to form a halogenated species **2**.[33] These molecules can then undergo cross-coupling reactions such as Sonogashira or Suzuki reactions using palladium catalysts (**Figure 5A**). With this approach, several 2,3-substituted NBDs **3** were synthesized.[11,20]

The second approach includes the use of cyclopentadiene (CP) **6** and substituted acetylene **7** in a [4+2] cycloaddition reaction, here a Diels-Alder reaction (**Figure 5B**). However, this electrocyclic reaction requires specific electronic properties of both reactants. Usually, it involves 4p-electrons of the diene and 2p-electrons of the dienophile. To match the electronic requirements, the HOMO of the diene and the LUMO of the dienophile need to overlap. This is even more favored when the dienophile carries an electron-withdrawing group (EWG, e.g. COR, COOR, CN) which facilitates the reaction by lowering the LUMO energy. Using the EWG group on the acetylene, the reaction with the reactive and electron-rich diene can be carried out easily, to result in NBDs **8**. Also, depending on the starting material this reaction can be performed neat, without involving any solvent. As shown previously, this synthesis route can be efficient for the preparation of various types of NBDs.[11] However, this approach also gives rise to challenges since the cyclopentadiene is unstable and usually forms an equilibrium with its dimer, dicyclopentadiene **9** (DCPD, **Cat. Nos. 8.03038** or **454338**). CP can be regained from DCPD **9** via a *retro* Diels-Alder reaction, through thermal cracking (**Figure 5C**). For NBDs requiring a higher temperature for synthesis, both reactions can be carried out in a combined fashion.

Most synthetic approaches were carried out in batches, which becomes impractical when upscaling is required. Therefore, another method gaining attention comes into play: flow chemistry. Recently, a continuous flow method that combines both the Diels-Alder and Cracking in one step was developed using a tubular flow reactor allowing for the preparation of larger quantities (**Figure 5D**).[34] Herein, a commercially available dienophile, ethyl phenylpropiolate (**Cat. No. E45309**), CP **6**, and DCPD **9**, were used for screening and optimization of the reaction in a 5 mL

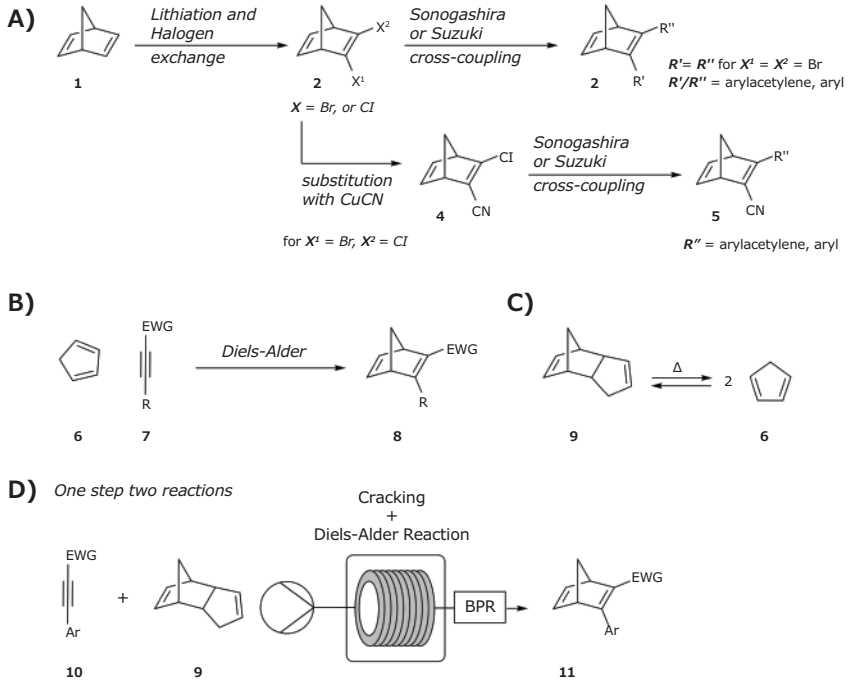

Figure 5. Synthetic approaches of norbornadienes as MOST material. A) Lithiation and Halogen exchange starting from norbornadiene, option for replacement of bromine with nitrile via substitution, and with subsequent cross-coupling reactions. B) Diels-Alder reaction between cyclopentadiene and activated acetylene. C) Dicyclopentadiene cracking to cyclopentadiene under thermal conditions. D) Recently developed combined cracking and Diels-Alder flow method to norbornadienes.

stainless steel coil reactor. Optimized conditions were then applied to various substituted acetylenes **10** to synthesize differently functionalized NBDs **11**. The method shows that it is possible to upscale and produce around 100 g of NBD in a few hours. Applications need larger amounts of material, which makes this method very valuable.

Azobenzene systems can be synthesized via various approaches.[35] The most common are Azo coupling and the Mills reaction. Azo coupling uses a diazonium salt as electrophile prepared from a primary amine with $NaNO_2$ (**Cat. No. 901903** or **563218**) in acidic media, and an electron-rich partner, such as arene derivatives decorated with electron-donating groups, while the Mills reaction includes a nitroso-derivative which is typically reacted with aniline in glacial acetic acid. DHA molecules have been prepared mainly through three pathways.[36] The first approach follows a [8+2] cycloaddition between 8-methoxyheptafulvene and dicyanoethylenes, the latter prepared from malononitrile (**Cat. No. M1407**) and carbonyl compounds. The second method directly starts from tropylium tetrafluoroborate (**Cat. No. 164623**) which either first reacts with a dicyanoethylene compound or a carbonyl derivative and then with malononitrile. This subsequently leads to the formation of a VHF molecule that reacts under heat to the corresponding DHA compound. The third route which primarily results in a substituted 7-membered ring relies on the utilization of tropone derivatives which forms the VHF, form but via condensation with dicyanoethylenes, which can then be converted to the DHA form using heat.

Energy Release in MOST Systems

MOST systems are unique energy systems in the sense that they offer energy capture, storage, and release in a single, emission-free system. The challenge is to design devices that make use of these attractive properties while mitigating challenges with low energy storage efficiency and energy density. In one implementation, a liquid MOST system is first pumped through a solar collector, and later, a heat release device containing a fixed bed catalytic system is used to trigger the heat release (**Figure 6A** left). In this way, chemical energy from the QC to NBD conversion was used to increase the temperature in the device from ambient temperature to 85 °C (**Figure 6A** right).[37] This heat release can also be used to heat water in a hybrid device (**Figure 6B**).[21] Electrochemistry can also be used to trigger heat release. In this way, the initial oxidation of QC leads to the conversion of several molecules by a local radical mechanism (**Figure 6C**).[38] Research shows this reaction works reversibly both in solution and in solid-state and offers an attractive way of controlling energy release.

Other systems feature hybrid combinations of MOST and phase change materials to allow for continuous thermal heat storage and release over extended periods (**Figure 6D**).[39] The co-location of the energy capture storage and release together with the semitransparency of most systems allows for unconventional applications, such as the possible integration of the MOST system into functional windows[40,41] where the MOST system is intended to regulate the daily variation of solar influx, where in many cases, strong solar influx at noon leads to strong heating, whereas energy loss through windows at night need heating (**Figure 6E**). A functional MOST system may in the future be used in this way to control indoor climates.

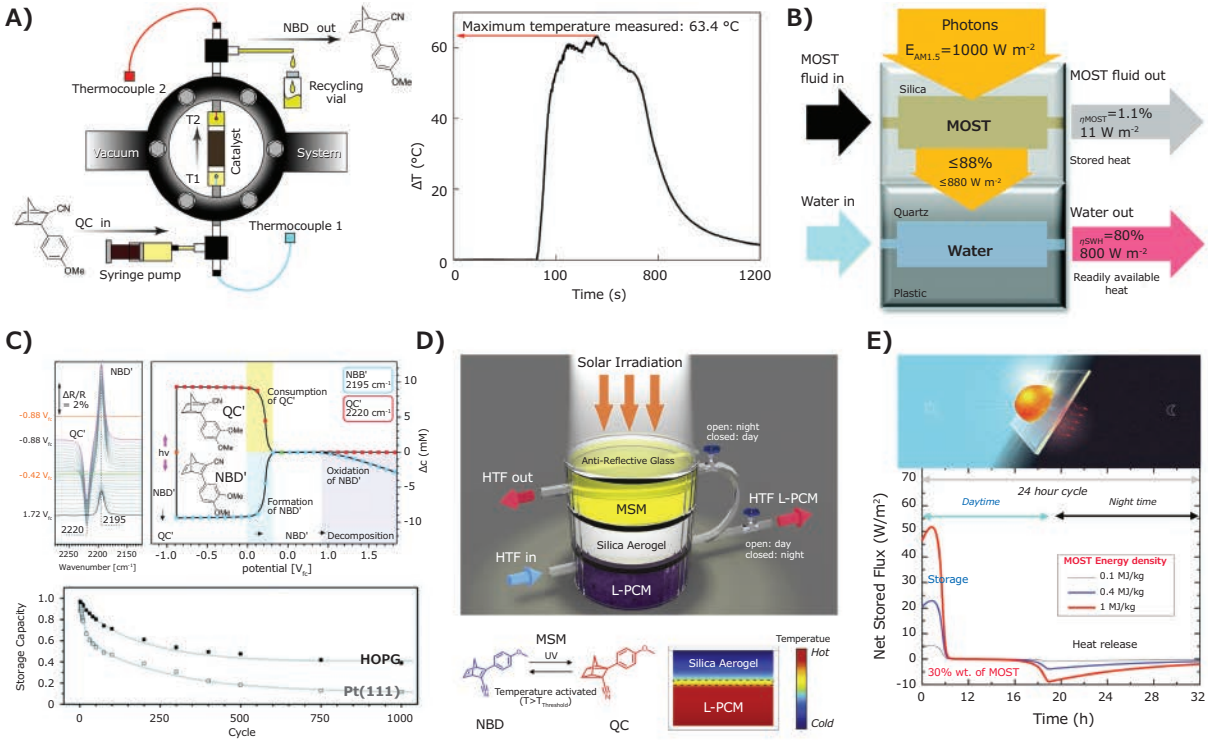

Figure 6. Examples of energy release and devices for conversion. A) Illustration of a heat release device and corresponding device plot. B) Illustration of a hybrid device used to heat water. C) Plots of energy conversion of several molecules by a local radical mechanism. D)Illustration of hybrid combinations of MOST and phase change materials allowing continuous thermal heat storage and release over time. E) Plot of a 24H cycle using MOST in a functional window. Figures reproduced from references 21, 37–39, 41, copyright The Royal Society of Chemistry 2019, The Royal Society of Chemistry 2017, The Royal Society of Chemistry 2020, 2019 Elsevier Inc., and 2022 by Elsevier Ltd.

Summary

MOST systems were first proposed for energy storage more than 100 years ago.[42] Recently, increased efforts have been carried out to improve the functionality of molecular photoswitches for solar energy storage. Herein we have introduced the features of MOST systems and presented design principles that have been used to increase energy storage density, efficiency, and availability, we have highlighted key examples of synthesis from literature. With increasing awareness of challenges with traditional energy production and geographic uneven distribution of fossil fuels, we hope that new, emission-free solar energy systems can be developed since the sun shines on all areas of the planet.

References

(1) (2019), I. E. A., World Energy Outlook 2019 (OECD)
(2) (2021), I. E. A., World Energy Outlook 2021 (OECD)
(3) Statistical Review of World Energy. BP Statistical Review of World Energy 2021, 70th ed Full report – Statistical Review of World Energy 2021 (bp.com)
(4) Ognjen S. Miljanic, J. A. P., Solar Energy. In Introduction to Energy and Sustainability, 1st ed.; Wiley-VCH: **2021**; pp 451–468.
(5) Wang, Z. et al. *Joule* **2021**, *5* (12), 3116–3136. DOI:10.1016/j.joule.2021.11.001.
(6) Dong, L. et al. *Chem. Soc. Rev.* **2018**, *47* (19), 7339–7368. DOI:10.1039/C8CS00470F.
(7) Bren, V. A. et al. *Russ. Chem. Rev.* **1991**, 60, 451–469. DOI:10.1070/RC1991v060n05ABEH001088.
(8) Börjesson, K. et al. *ACS Sustain. Chem. Eng.* **2013**, *1* (6), 585–590. DOI:10.1021/sc300107z.
(9) Orrego-Hernández, J. et al. *Acc. Chem. Res.* **2020**, *53* (8), 1478–1487. DOI:10.1021/acs.accounts.0c00235.
(10) Lennartson, A. et al. *Tetrahedron Lett.* **2015**, *56* (12), 1457–1465. DOI:10.1016/j.tetlet.2015.01.187.
(11) Jevric, M. et al. *Chem. Eur. J.* **2018**, *24* (49), 12767–12772. DOI:10.1002/chem.201802932.
(12) Taoda, H. et al. *J. Chem. Eng. Jpn.* **1987**, *20* (3), 265–270. DOI:10.1252/jcej.20.265.
(13) Wang, Z. et al. *Adv. Sci.* **2021**, *8* (21), 2103060. DOI:10.1002/advs.202103060.
(14) He, Y. et al. *Angew. Chem. Int. Ed.* **2021**, *60* (30), 16539–16546. DOI:10.1002/anie.202103705.
(15) Broman, S. L.; Nielsen, M. B. *Phys. Chem. Chem. Phys.* **2014**, *16* (39), 21172–21182. DOI:10.1039/C4CP02442G.
(16) Yoshida, Z.-i. *J. Photochem.* **1985**, *29* (1), 27–40. DOI:10.1016/0047-2670(85)87059-3.
(17) Mansø, M. et al. *Org. Biomol. Chem.* **2018**, *16* (31), 5585–5590. DOI:10.1039/C8OB01470A.
(18) Mansø, M. et al. *Nat. Commun.* **2018**, *9* (1), 1945. DOI:10.1038/s41467-018-04230-8.
(19) Gray, V. et al. *Chem. Commun.* **2014**, *50* (40), 5330–5332. DOI:10.1039/C3CC47517D.
(20) Quant, M. et al. *Chem. Eur. J.* **2016**, *22* (37), 13265–74. DOI:10.1002/chem.201602530.
(21) Dreos, A. et al. *Energy Environ. Sci.* **2017**, *10* (3), 728–734. DOI:10.1039/C6EE01952H.
(22) Jorner, K. et al. *J. Mater. Chem. A* **2017**, *5* (24), 12369–12378. DOI:10.1039/C7TA04259K.
(23) Kuntze, K. et al. *Photochem. Photobiol. Sci.* **2022**, *21* (2), 159–173. DOI:10.1007/s43630-021-00145-4.
(24) Fang, D. et al. *J. Am. Chem. Soc.* **2021**, *143* (36), 14502–14510. DOI:10.1021/jacs.1c08704.
(25) Shi, Y. et al. *J. Mater. Chem. A* **2021**, *9* (15), 9798–9808. DOI:10.1039/D1TA01007G.
(26) Broman, S. L. et al. *Chem. Eur. J.* **2013**, *19* (29), 9542–9548. DOI:10.1002/chem.201300167.
(27) Kilde, M. D. et al. *Eur. J. Org. Chem.* **2017**, *2017* (6), 1052–1062. DOI:10.1002/ejoc.201601435.
(28) Mogensen, J. et al. *Eur. J. Org. Chem.* **2019**, 2019 (10), 1986–1993. DOI:10.1002/ejoc.201801776.
(29) Cacciarini, M. et al. *Chem. Eur. J.* **2015**, *21* (20), 7454–7461. DOI:10.1002/chem.201500100.
(30) Skov, A. B. et al. *Chem. Eur. J.* **2016**, *22* (41), 14567–14575. DOI:10.1002/chem.201601190.

(31) Kenndoff, J. et al. *J. Am. Chem. Soc.* **1990**, *112* (16), 6117–6118. DOI:10.1021/ja00172a031.
(32) Tranmer, G. K. et al. *Can. J. Chem.* **2000**, *78* (5), 527–535. DOI:10.1139/v00-047.
(33) Lennartson, A. et al. *Synlett* **2015**, *26* (11), 1501–1504. DOI:10.1055/s-0034-1380417.
(34) Orrego-Hernández, J. et al. *Eur. J. Org. Chem.* **2021**, *2021* (38), 5337–5342. DOI:10.1002/ejoc.202100795.
(35) Merino, E. *Chem. Soc. Rev.* **2011**, *40* (7), 3835–3853. DOI:10.1039/C0CS00183J.
(36) Lubrin, N. C. M. et al. *Eur. J. Org. Chem.* **2017**, *2017* (20), 2932–2939. DOI:10.1002/ejoc.201700446.
(37) Wang, Z. et al. *Energy Environ. Sci.* **2019**, *12* (1), 187–193. DOI:10.1039/C8EE01011K.
(38) Waidhas, F. et al. *J. Mater. Chem. A* **2020**, *8*, 15658–15664. DOI:10.1039/D0TA00377H.
(39) Kashyap, V. et al. *Joule* **2019**, *3* (12), 3100–3111. DOI:10.1016/j.joule.2019.11.001.
(40) Petersen, A. U. et al. *Adv. Sci.* **2019**, *6* (12), 1900367. DOI:10.1002/advs.201900367.
(41) Refaa, Z. et al. *Appl. Energy* **2022**, *310*, 118541. DOI:10.1016/j.apenergy.2022.118541.
(42) Weigert, F. *Berichte der deutschen chemischen Gesellschaft* **1909**, *42* (1), 850–862. DOI:10.1002/cber.190904201136.

Materials for MOST

Name	Form	Description	Cat. No.
Cerium(IV) oxide	20 wt. % colloidal dispersion in 2.5% acetic acid	30-50 nm avg. part. size	**289744-500G**
	nanoparticle dispersion, 10 wt. % in H_2O	<25 nm particle size	**643009-100ML**
	nanopowder	<25 nm particle size (BET)	**544841-5G** **544841-25G**
		<50 nm particle size (BET) 99.95% trace rare earth metals basis	**700290-25G** **700290-100G**
	powder	<5 µm, 99.9% trace metals basis	**211575-100G** **211575-500G**
		99.995% trace metals basis	**202975-10G** **202975-50G**
	solid	≥99.0%	**22390-100G-F**
Cerium(IV) oxide-gadolinium doped	nanopowder, contains 10 mol % gadolinium as dopant	<500 nm particle size	**572330-25G**
	nanopowder, contains 20 mol % gadolinium as dopant	<100 nm particle size	**572357-25G**
Cerium(IV)-zirconium(IV) oxide	nanopowder	<50 nm particle size (BET) 99.0% trace metals basis	**634174-25G** **634174-100G**
Lanthanum strontium cobalt ferrite	powder	composite cathode powder, LSCF/GDC	**704253-10G**
		LSCF 6428	**704288-10G**
Lanthanum strontium manganite	powder	LSM-20, ≥99%	**704296-10G**
		LSM-35	**704261-10G**
	solid	composite cathode powder, LSM-20/GDC10	**704237-10G**
Nickel(II) oxide	nanopowder	<50 nm particle size (TEM) 99.8% trace metals basis	**637130-25G** **637130-100G** **637130-250G**
	powder	-325 mesh, 99%	**399523-100G**
	powder and chunks	99.99% trace metals basis	**203882-20G** **203882-100G**
	solid	≥99.995% trace metals basis	**481793-5G** **481793-25G**
Strontium oxide	powder	99.9% trace metals basis	**415138-10G** **415138-50G**
Strontium peroxide	powder	98%	**415200-100G**
Vanadium(III) oxide	powder and chunks	99.99% trace metals basis	**463744-5G** **463744-25G**
Vanadium(V) oxide	powder	99.95% trace metals basis	**204854-1G** **204854-5G** **204854-25G**
Yttrium(III) oxide	nanopowder	<50 nm particle size	**544892-25G**
	powder	99.99% trace metals basis	**205168-10G** **205168-50G** **205168-250G**
		99.999% trace metals basis	**204927-10G** **204927-50G**
	nanoparticle dispersion 10 wt. % in isopropanol	<100 nm (DLS) ≥99.9% trace metals basis	**702048-100G**
Zirconium(IV) oxide-yttria stabilized	nanopowder	≤100 nm particle size	**572322-25G**
	nanopowder contains 8 mol % yttria as stabilizer	<100 nm particle size	**572349-25G**
	powder	<100 nm particle size	**544779-25G**
	submicron powder	99.9% trace metals basis (purity excludes ~2% HfO_2)	**464228-100G** **464228-500G**

R&D Highlight

2D Layered Perovskites

Solution Processable Materials

The recent discovery that single-layer 2D perovskites can be prepared using solution processing techniques[1] has been followed by enormous research into optoelectronic applications of 2D perovskites including light emitting diodes (LEDs),[2] phototransistors,[3] and solar cells,[4] and lasers.[5]

Direct and Tunable Bandgap

Photoluminescent 2D perovskites have a direct bandgap with a narrow emission peak that changes depending on the layer thickness and the choice of amine and halide. We offer an excellent portfolio of the most popular 2D perovskite compositions for photoluminescence based devices.

Improved Moisture Stability

Solar cells fabricated with 2D perovskites have improved stability in moist air compared to 3D perovskites.[4]

Formula	Cat. No.	Layer Thickness	$(RNH_3)_2(MeNH_3)_{n-1}\ Pb_nX_{3n+1}$		
			R	X	n
$(BA)_2PbI_4$	**910961**	n=1	Bu	I	1
$(BA)_2PbBr_4$	**910953**	n=1	Bu	Br	1
$(PEA)_2PbI_4$	**910937**	n=1	PE	I	1
$(PEA)_2PbBr_4$	**910945**	n=1	PE	Br	1
$(BA)_2(MA)Pb_2I_7$	**912816**	n=2	Bu	I	2
$(BA)_2(MA)_2Pb_3I_{10}$	**912557**	n=3	Bu	I	3
$(BA)_2(MA)_3Pb_4I_{13}$	**914363**	n=4	Bu	I	4
$(BA)_2(MA)_4Pb_5I_{16}$	**912301**	n=5	Bu	I	5

BA = n-butylammonium; PEA = 2-phenylethylammonium;
MA =methylammonium, Bu=n-butyl, PE=2-phenylethyl

SigmaAldrich.com/perovskite

References:

1) Dou, L.; Wong, A. B.; Yu, Y.; Lai, M.; Kornienko, N.; Eaton, S. W.; Fu, A.; Bischak, C. G.; Ma, J.; Ding, T.; Ginsberg, N. S.; Wang, L-W.; Alivisatos, A. P.; Yang, P. *Science* **2015,** *349,* 1518. DOI: 10.1126/science.aac7660

2) Yuan, M.; Quan, L. N.; Comin, R.; Walters, G.; Sabatini, R.; Voznyy, O.; Hoogland, S.; Zhao, Y.; Beauregard,E. M.; Kanjanaboos, P.; Lu, Z.; Kim, D. H.; Sargent, E. H. *Nat. Nanotechnol.* **2016,** *11,* 872. DOI: 10.1038/NNANO.2016.110

3) Shao, Y.; Liu, Y.; Chen, X.; Chen, C.; Sarpkaya, I.; Chen, Z.; Fang, Y.; Kong, J.; Watanabe, K.;Taniguchi, T.; Taylor, A.; Huang, J.; Xia, F. *Nano Lett.* **2017,** *17,* 7330. DOI: 10.1021/acs.nanolett.7b02980

4) Cao, D. H.; Stoumpos, C. C.; Farha, O. K.; Hupp, J. T.; Kanatzidis, M. G. *J. Am. Chem.* Soc. **2015,** *137,* 7843. DOI: 10.1021/jacs.5b03796

5) Raghavan, C. M.; Chen, T.-P.; Li, S.-S.; Chen, W.-L.; Lo, C.-Y.; Liao, Y.-M.; Haider, G.; Lin, C.-C.; Chen, C.-C.; Sankar, R.; Chang, Y.-M.; Chou, F.-C.; Chen, C.-W. *Nano Lett.* **2018**, *18* (5), 3221. DOI: 10.1021/acs.nanolett.8b00990

Nanostructured Catalyst for Direct Alcohol Low-Temperature Fuel Cells



Priscilla J. Zambiazi, and Rodrigo F.B. de Souza, Almir Oliveira Neto*

Instituto de Pesquisas Energéticas e Nucleares, IPEN/CNEN-SP, Av. Prof. Lineu Prestes, 2242 Cidade Universitária, CEP 05508-900 São Paulo, SP, Brazil
* Email: aolivei@usp.br

Introduction

At a time when the world is committed to changing its energy matrix, fuel cells are back on the scene as a promising source of energy. Fuel cells can convert chemical energy into electrical energy efficiently. Conceptually, fuel cells are very similar to the Daniell cell, which is often taught in introductory chemistry courses. In a Daniell cell, the anode (usually a metal like zinc) is oxidized and the oxidized metal ions dissolve into the electrolytic solution while metal ions at the cathode surface are reduced. Similarly, in a fuel cell, molecules (for example, H_2 and O_2) are inserted into the device and are oxidized and reduced at the electrodes.[1]

Conceptually, the hydrogen fuel cell is one of the cleanest energy sources, consuming only hydrogen and oxygen and releasing only water; however, hydrogen fuel cells face technological challenges. For example, producing, storing, and transporting hydrogen is still expensive and incurs considerable risks, even though the technology to accomplish these processes has greatly evolved. In addition, the loss of gas during storage and transport remains a challenge.[2]

One strategy to overcome this problem was the adoption of hydrogen-generating devices, such as thermo-reformers, to generate hydrogen on demand for use in the fuel cell.[3–4] The downside to this strategy is that the power generation system occupies more volume due to this extra device.

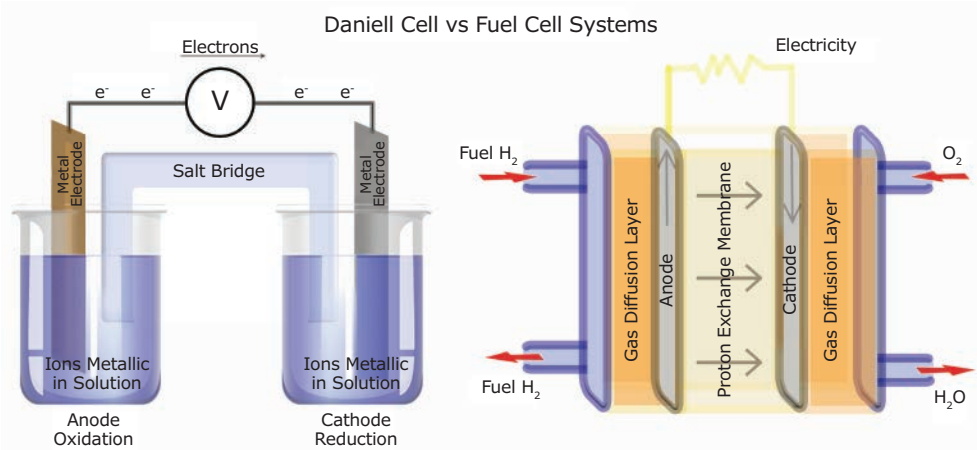

Figure 1. Diagram of the Daniell Cell and the Hydrogen Fuel Cell devices.

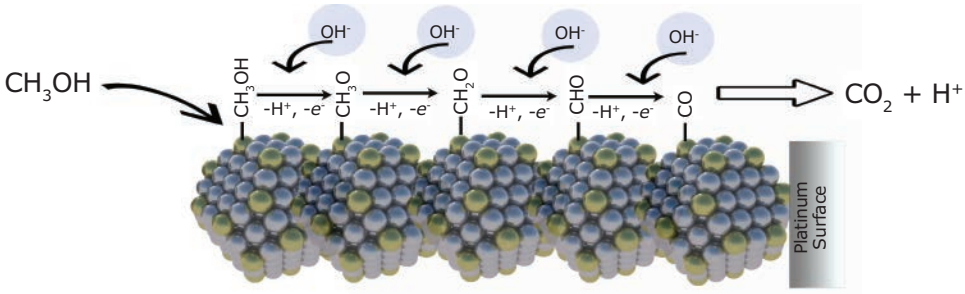

Figure 2. Bifunctional mechanism of the methanol oxidation on the platinum surface catalyst.

Direct Alcohol Fuel Cells

Among the possibilities of fuels of a PEM-FC, alcohols are the most deeply studied, the main ones being methanol, ethanol, and glycerol.

Direct Methanol Fuel Cells

Direct alcohol oxidation cells started with the simplest alcohol, methanol, which is a liquid that is easy and cheap to store and transport, and has a high energy density of 6.09 kWh kg^{-1}, including an existing distribution network due to being an industrial input.[5] Initial studies identified platinum (Pt) as a promising catalyst for the methanol oxidation reaction (MOR), but two main obstacles quickly emerged: 1) Pt is expensive and 2) Pt in MOR is prone to poisoning by carbon monoxide.

Fortuitously, the beginning of studies on the methanol oxidation reaction (MOR) happened concomitantly with the development of new methods for preparing nanostructured materials. Researchers found that nanostructured materials as catalysts for MOR may offer a solution to both of the obstacles faced by traditional Pt catalysts. The findings on nanostructure platinum galvanized interest in studying direct methanol fuel cells (DMFC). One strategy that emerged to address the catalytic poisoning was to use reactive oxygen species (ROS), made by the water activation product, to constantly remove some of this catalytic poison. A second strategy, adopted from research on the electrolysis reaction, soon followed, to add other metals such as ruthenium (Ru) together with Pt that would act in a bifunctional mechanism (**Figure 2**). In this mechanism, the ROS reacts with the strongly adsorbed CO on the electrode surface oxidizing it to CO2.[6]

During this period, not only the addition of a second, sometimes a third, and even a fourth metal was studied, but also the optimal composition, which, in addition to increasing the activity of the catalyst, also reduced the use of platinum in the catalyst. One particularly successful catalyst developed in this period is PtRu in the composition 50% in atoms among the metals, which to this day is still considered the benchmark for MOR, even though superior materials have already been presented in the literature.[6]

Researchers developed another way to obtain ROS for CO removal, by adding rare earth oxides to the catalyst. These rare earth oxides, such as ceria, act as an oxygen buffer near the surface of the material. By changing its oxidation state easily according to the presence or absence of oxygen near its interface, ceria creates a chemical environment on the electrode surface that favors CO oxidation.[7]

Yet another approach is to tailor the Pt catalyst. For example, changing the platinum D-band density decreases the CO adsorption energy and limits catalytic poisoning. This strategy is based on the insertion of a metallic heteroatom in the crystalline structure of platinum, obtaining alloys, the named electronic effect.[8] The CO oxidation at low overpotentials can also be achieved by selecting preferred platinum faces, for example, low-index crystalline planes, which have adequate surface energy to carry out the oxidation of CO and water at low overpotentials. Similarly, the same effect can be obtained by creating surface defects as reported by Ramos et al.[9]

Direct Ethanol Fuel Cell

Studies with alcohols have expanded to the oxidation of ethanol, as a substitute for methanol, because it is less toxic, has an energy density greater than that of methanol (8.02 kWh kg^{-1}), and mainly to be a renewable fuel obtained from biomass. The use of alcohol with a slightly longer chain brought with it the problems of methanol and a new challenge, the breaking of the C-C bond. Pt-based electrocatalysts were not efficient for this purpose; however, the alloy PtSn 3:1 was appointed as the benchmark due to the high powers obtained.[10]

Even the PtSn alloy does not show the complete oxidation of alcohol to CO_2, and in search of these scientists began a new search for solutions that could help to overcome this challenge. One of the options found was the addition of Rh to the catalyst because this metal has an electron affinity for the C-C bond.[11] However, studies that explored this option showed only an increase in CO_2 generation, but this was reflected in smaller currents. This fact combined with the high costs of Rh reduced the use of this noble metal as the catalyst for the ethanol oxidation reaction.

Another strategy adopted was the use of catalysts with steps and terraces to break the C-C bond. However, these stepped and terraced materials tend to restructure to more stable forms, which makes it difficult to maintain the effect in the long term. In addition, stepped and terraced materials are difficult to synthesize, which discourages the application of this kind of material on a large scale.

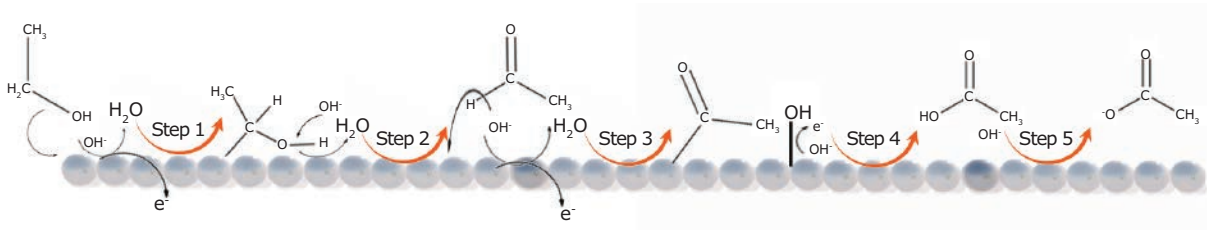

Figure 3. Schematic representation of the pathways of ethanol oxidation on the metallic catalytic surface.

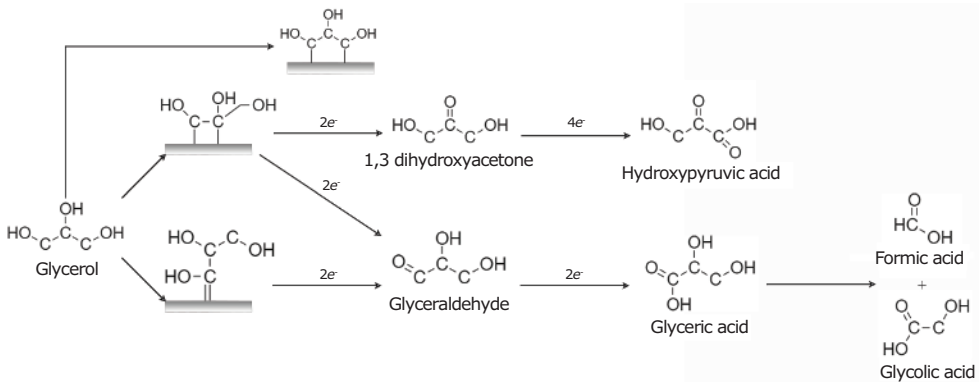

Figure 4. Reaction mechanism of glycerol oxidation in an acidic environment to produce different products.

One of the additional challenges that ethanol brings is that the partial oxidation of ethanol yields stable products like acetaldehyde and acetic acid. On the one hand, the incomplete oxidation of ethanol reduces the energy density that can be utilized, which is a drawback, but on the other hand, these products do not strongly adsorb to the catalyst and do not function as catalytic poisons. The most active catalysts for the ethanol oxidation reaction normally affect the kinetics of acetaldehyde or acetic acid formation, which can go through several oxidation pathways[12] as shown in **Figure 3**. To date, catalyzing the partial oxidation of ethanol is much better understood than the slow step of breaking the C-C bond.

Direct Glycerol Fuel Cell

With the popularization of biodiesel, the production of glycerol grew beyond what the market needed, transforming this alcohol from a commodity to an environmental problem. Being another fuel from biomass, this alcohol with its three hydroxyls has the breaking of the C-C bond facilitated by the steric effect of the oxidation of any of the three functional groups, but, like methanol, it has similar problems with CO.

Usually, the potency densities obtained by the oxidation of glycerol are lower than those of the other alcohols already presented, but the diversity of products formed during the oxidation of glycerol opened the eyes of the scientific community to the possibilities of co-generation of energy and chemicals.[13] **Figure 4** shows the reaction pathways of glycerol oxidation.[14]

Anion Exchange Membrane Fuel Cells

Around 2010 the development of anion exchange membranes brought the possibility of carrying out the oxidation of alcohols in an alkaline medium and with that some advantages, such as greater ease in the oxidation of alcohols whose hydroxyls are more easily deprotonated, the alkaline medium also reduces the possibility of intermediates to be formed during oxidation. Since aldehydes are unstable at high pH and most importantly, many metals that only activate water at neutral pHs become active at high pH in the oxidation of alcohols. One such metal is Pd, which is around 30 times more abundant than platinum. Other transition metals also appeared as viable, such as Ni, Cu, Au, Ag.[15]

Studies on the oxidation of alcohols in the alkaline medium have gone into great depth in the last few decades, but anion exchange membranes have not evolved at the same rate as catalysis, and are still not very durable.[16] The alkaline medium suffers from another type of catalytic poisoning, the coverage of the site by the deposition of solid carbonate deposited on the catalytic layer, this carbonate from the precipitation of CO and CO_2 in an alkaline medium prevents the arrival of new alcohol molecules to the catalytic surface.

Opportunities and Outlook

Nanostructured materials made it possible to study low-temperature fuel cells, especially those fueled with alcohol, which brings the possibility of obtaining renewable energy from alcohols such as ethanol and glycerol. Anion exchange membranes brought the possibility of decreasing the dependence of Pt on the catalyst, but they need to evolve to increase durability.

Regardless of cell type, for ethanol and glycerol, the most active catalysts are not those that promote complete oxidation of alcohol, which implies a lower use of energy density, however, makes it possible to obtain chemically stable partially oxidized products. This allows the cells to do something beyond their initial purpose of generating energy, but rather the co-generation of energy and chemicals.

References

(1) Brusso, B. C. *IEEE Ind. Appl. Mag.* **2021**, *27* (5), 8–13. DOI: 10.1109/MIAS.2021.3086965.

(2) Singla, M. K.; Nijhawan, P.; Oberoi, A. S. *Environ. Sci. Pollut. Res.* **2021**, *28* (13), 15607-15626. DOI:10.1007/s11356-020-12231-8. Wu, W.; Pai, C.-T.; Viswanathan, K.; Chang, J.-S. *J. Clean. Prod.* **2021**, *300*, 126959. DOI:10.1016/j.jclepro.2021.126959.

(3) Boettner, D. D.; Moran, M. J. Proton exchange membrane (PEM) fuel cell-powered vehicle performance using direct-hydrogen fueling and on-board methanol reforming. Energy 2004, 29 (12), 2317-2330. DOI:10.1016/j.energy.2004.03.026.

(4) Assumpção, M. H. M. T.; Piasentin, R. M.; Hammer, P.; De Souza, R. F. B.; Buzzo, G. S.; Santos, M. C.; Spinacé, E. V.; Neto, A. O.; Silva, J. C. M. *Appl. Catal.* **2015**, *174–175*, 136–144. DOI:10.1016/j.apcatb.2015.02.021. Nandenha, J.; Fontes, E. H.; Piasentin, R. M.; Fonseca, F. C.; Neto, A. O. *J. Fuel Chem. Technol.* **2018**, *46* (9), 1137–1145. DOI:10.1016/S1872-5813(18)30046-X. Braesch, G.; Wang, Z.; Sankarasubramanian, S.; Oshchepkov, A. G.; Bonnefont, A.; Savinova, E. R.; Ramani, V.; Chatenet, M. *J. Mater. Chem. A* **2020**, *8* (39), 20543–20552, 10.1039/D0TA06405J. DOI:10.1039/D0TA06405J.

(5) Ai, T.; Bao, S.; Lu, J. *Front. Chem.* **2021**, *9*. DOI:10.3389/fchem.2021.667754.

(6) Lu, S.; Li, H.; Sun, J.; Zhuang, Z. *Nano Res.* **2018**, *11* (4), 2058–2068. DOI:10.1007/s12274-017-1822-x.

(7) Wang, Q.; Liu, Z.; An, S.; Wang, R.; Wang, Y.; Xu, T. *J. Rare Earths* **2016**, *34* (3), 276–282. DOI:10.1016/S1002-0721(16)60025-X.

(8) Lu, C.; Lee, I. C.; Masel, R. I.; Wieckowski, A.; Rice, C. *J. Phys. Chem. A* **2002**, *106* (13), 3084–3091. DOI:10.1021/jp0136359.

(9) Ramos, A. S.; Santos, M. C. L.; Godoi, C. M.; de Queiroz, L. C.; Nandenha, J.; Fontes, E. H.; Brito, W. R.; Machado, M. B.; Neto, A. O.; de Souza, R. F. B. *Int. J. Hydrog. Energy* **2020**, *45* (43), 22973–22978. DOI:10.1016/j.ijhydene.2020.06.105.

(10) De Souza, R. F. B.; Parreira, L. S.; Rascio, D. C.; Silva, J. C. M.; Teixeira-Neto, E.; Calegaro, M. L.; Spinace, E. V.; Neto, A. O.; Santos, M. C. *J. Power Sources* **2010**, *195* (6), 1589–1593. DOI:10.1016/j.jpowsour.2009.09.065.

(11) Bai, J.; Xiao, X.; Xue, Y.-Y.; Jiang, J.-X.; Zeng, J.-H.; Li, X.-F.; Chen, Y. *ACS Appl. Mater. Interfaces* **2018**, *10* (23), 19755–19763. DOI:10.1021/acsami.8b05422.

(12) Marinkovic, N. S.; Li, M.; Adzic, R. R. *Top. Curr. Chem.* **2019**, *377* (3), 11. DOI:10.1007/s41061-019-0236-5.

(13) Fontes, E. H.; Ramos, C. E. D.; Ottoni, C. A.; de Souza, R. F. B.; Antolini, E.; Neto, A. O. *Renew. Energ.* **2021**, *167*, 954–959. DOI:10.1016/j.renene.2020.12.026.

(14) Liang, Z.; Villalba, M. A.; Marcandalli, G.; Ojha, K.; Shih, A. J.; Koper, M. T. M. *ACS Catal.* **2020**, *10* (23), 13895–13903. DOI:10.1021/acscatal.0c04131.

(15) Fontes, E. H.; Piasentin, R. M.; Ayoub, J. M. S.; da Silva, J. C. M.; Assumpção, M. H. M. T.; Spinacé, E. V.; Neto, A. O.; de Souza, R. F. B. *Mater. Renew. Sustain. Energy* **2015**, *4* (1), 3. DOI:10.1007/s40243-015-0043-z.

(16) Dekel, D. R. *J. Power Sources* **2018**, *375*, 158-169. DOI:10.1016/j.jpowsour.2017.07.117.

Proton Exchange Membrane (PEM) Fuel Cells

Name	Form	Description	Cat. No.
Aquivion® D83-06A	20% dispersion in water	6% polymer content in lower aliphatic alcohols and water	**802603-50ML** **802603-500ML**
Aquivion® D83-24B	24% dispersion in water	PFSA eq. wt. 830 g/mole SO_3H	**802654-25ML** **802654-250ML**
Aquivion® D72-25BS	25% dispersion in water	PFSA eq. wt. 720 g/mole SO_3H stabilized CF_3 polymer chain ends	**802549-25ML** **802549-250ML**
Aquivion® D79-25BS		PFSA eq. wt. 790 g/mole SO_3H contains CF_3 polymer chain ends as stabilizer	**802565-25ML** **802565-250ML**
Aquivion® D79-25BS-Li		PFSLi eq. wt. 790 g/mole SO_3Li stabilized CF_3 polymer chain ends	**802573-25ML**
Aquivion® D98-25BS		PFSA eq. wt. 980 g/mole SO_3H contains CF_3 polymer chain ends as stabilizer	**802557-25ML** **802557-250ML**
Aquivion® P87S-SO2F	2mm cylindrical pellets	PFSF eq. wt. (870 g/mole SO_2F) contains CF_3 polymer chain ends as stabilizer	**802530-50G**
Aquivion® P98-SO2F		PFSF eq. wt. 980 g/mole $SO_2$2F	**802662-50G**
Aquivion® pellets P87-SO2F		PFSF eq. wt. 870 g/mole SO_2F	**915327-50G**
Aquivion® PW79S	coarse powder	PFSA eq. wt. 790 g/mole SO_3H contains CF_3 polymer chain ends as stabilizer	**802611-25G**
Aquivion® PW79S-Li		PFSA eq. wt. 790 g/mole SO_3Li stabilized CF_3 polymer chain ends	**802581-10G**
Aquivion® PW87S		PFSA eq. wt. 870 g/mole SO_3H contains CF_3 polymer chain ends as stabilizer	**802646-25G**
Aquivion® PW98		PFSA eq. wt. 980 g/mole SO_3H	**802638-25G**
Disodium bis(4-chloro-3-sulfophenyl)sulfone	crystals	97%	**730882-5G**
Platinum on silica	granular	extent of labeling: 1 wt. % loading	**520691-25G** **520691-100G**
Poly(2-vinylpyridine-co-styrene)		average M_n ~130,000 average M_w ~220,000 by LS, granular	**184608-50G**
Aquivion® E98-05S	membrane sheet, L x W 31 cm x 31 cm	contains CF_3 polymer chain ends as stabilizer PFSA eq. wt. 980 g/mole SO_3H	**802700-1EA**
Aquivion® E87-12S	membrane sheet, L x W x thickness 18 cm x 18 cm x 120 µm	contains CF_3 polymer chain ends as stabilizer PFSA eq. wt. 870 g/mole SO_3H	**802786-1EA**
Aquivion® E98-15S	membrane sheet, L x W x thickness 18 cm x 18 cm x 150 µm	stabilized CF_3 polymer chain ends PFSA eq. wt. 980 g/mole SO3H	**802751-1EA**
Aquivion® E87-05S	membrane sheet, L x W x thickness 18 cm x 18 cm x 50 µm	contains CF_3 polymer chain ends as stabilizer PFSA eq. wt. 870 g/mole SO_3H	**8027191EA**
Aquivion® E98-05		PFSA eq. wt. 980 g/mole SO_3H	**802670-1EA**

Name	Form	Description	Cat. No.
Aquivion® E98-09S	membrane sheet, L x W x thickness 18 cm x 18 cm x 90 µm	contains CF_3 polymer chain ends as stabilizer PFSA eq. wt. 980 g/mole SO_3H	**802735-1EA**
Aquivion® E87-12S	membrane sheet, L x W x thickness 31 cm x 31 cm x 120 µm	stabilized CF_3 polymer chain ends PFSA eq. wt. 870 g/mole SO_3H	**802514-1EA**
Aquivion® E98-15S	membrane sheet, L x W x thickness 31 cm x 31 cm x 150 µm	contains CF_3 polymer chain ends as stabilizer PFSA eq. wt. 980 g/mole SO_3H	**802778-EA**
Aquivion® E87-05	membrane sheet, L x W x thickness 31 cm x 31 cm x 50 µm	PFSA eq. wt. 870 g/mole SO_3H	**915866-1EA**
Aquivion® E87-05S		contains CF_3 polymer chain ends as stabilizer PFSA eq. wt. 870 g/mole SO_3H	**802727-1EA**
Aquivion® E98-05		PFSA eq. wt. 980 g/mole SO_3H	**802697-1EA**
Aquivion® E98-09S	membrane sheet, L x W x thickness 31 cm x 31 cm x 90 µm	contains CF_3 polymer chain ends as stabilizer PFSA eq. wt. 980 g/mole SO_3H	**802743-1EA**
Platinum black	powder	fuel cell grade, ≥99.9% trace metals basis	**520780-1G** **520780-5G**
Platinum cobalt on carbon		extent of labeling: 30 wt. % Pt3Co loading	**738565-1G**
Platinum on graphitized carbon		extent of labeling: 10 wt. % loading	**738581-1G**
Platinum on graphitized carbon		extent of labeling: 20 wt. % loading	**738549-1G**
Platinum on graphitized carbon		extent of labeling: 40 wt. % loading	**738557-1G**
Platinum-ruthenium alloy on graphitized carbon		extent of labeling: 20 wt. % Pt loading extent of labeling:10 wt. % Ru loading	**738573-1G**
Poly(vinylphosphonic acid)			**661740-1G**

How to Best Store Electrical Energy

Ulrich Stimming*

Chemistry - School of Natural and Environmental Sciences, Newcastle University, Newcastle upon Tyne NE1 7RU, United Kingdom
*Email: Ulrich.Stimming@newcastle.ac.uk

Advantages of Electrochemical Systems

Historically, energy storage to power vehicles and electrical grids has relied on converting chemical energy to mechanical and electrical energy by a heat process using the Carnot cycle. This process often involves burning fossil fuels to generate heat and converting heat to mechanical energy, as in a typical heat engine. Unfortunately, this process is inefficient, as shown by the maximum theoretical efficiency of only 64% and actual efficiencies only at 30-40%. In addition, burning fossil fuels generates environmentally damaging waste products, including CO_2, methane, and nitrous oxide. Consequently, scientists have sought more efficient and cleaner energy storage and conversion processes.

Electrochemical systems have tremendous promise for storing energy and converting energy to workable forms. Efficiencies of electrochemical systems typically can be 40-60% and even greater than 85% in newer technologies. In addition, some electrochemical systems, like the polyoxometalate-based redox-flow batteries discussed here, operate with a near 100% atom economy and operate without generating any chemical waste directly. These aspects give electrochemical systems an advantage compared to heat engines.

Advances in Fuel Cells

One promising type of electrochemical system is the hydrogen-based fuel cell. Assuming hydrogen as a fuel, fuel cells can offer high efficiencies for electricity production of 50–60% compared to a heat engine of 30–40%. Current stack operations yield power densities of 6kW/L and more. If goals of 1 W/cm^2 @0.8V (single cell) become feasible, the efficiencies will be pushed to 70–80%.

Hydrogen-based fuel cells are very attractive for energy conversion because they are much more efficient and environmentally cleaner than heat engines. Still, hydrogen-based fuel cells do have limitations for energy storage. First, using hydrogen as an energy storage medium means converting electricity to hydrogen and back to electricity. Because this involves two conversions with losses at each conversion, the efficiency of the storage process drops to only 35–45%. Second, hydrogen fuel cells are expensive. Hydrogen fuel needs specific storage conditions, such as high-pressure tanks and/or cryogenic temperatures. Building hydrogen storage at scale requires significant capital investment considering the components, the electrolyzer, the fuel cell, and other components. Third, hydrogen is highly flammable, which poses safety hazards. The flammability, combined with the difficulties of storing hydrogen, significantly limits the use of hydrogen as a mobile fuel.

Alternatives: Li-Ion and Other Concepts

An alternative electrochemical system, a battery, is much better suited to energy storage. Typical battery storage efficiencies, including the entire cycle, are around 80%, nearly double that of today's hydrogen fuel cell. Two battery systems, among many more, should be briefly mentioned here. The Li-ion battery has become quite ubiquitous because of its excellent properties. These batteries are used in portable electronics, automotive applications, and stationary purposes. For example, a Li-ion battery of 85kWh in a Tesla Model S car has a volume and weight of 263 L and 400 kg, respectively (excluding protective housing, BMS, and power conditioning), which can yield a range of up to 450 km.

But Li-ion batteries have downsides: One downside of the Li-ion battery is that the raw materials used in the battery are available only in a few countries (similar to oil) with all the polito-economic consequences associated. Another downside is that the battery lifetime (load/unload cycles) is short, and methods to recycle the valuable battery components are still in their infancy. In addition, technical improvements, like the faster charge-discharge rate and increased gravimetric capacity, are needed. One notable downside of lithium-ion batteries is their safety. Under certain operation conditions, but also in standby mode, a thermal run-away can occur, or by other adverse conditions, the batteries can burn

or even explode. Many incidents have been described. Recently an ocean freighter bringing electric cars from Europe to North America burned out and sank, with steel walls melting in the high heat of the fire induced by the Li-ion batteries.

Another type of battery is the redox flow battery (RFB). A redox flow battery, like any battery, converts chemical energy to electrical energy. In a redox flow battery, two solution-phase chemical components are pumped passed current collecting electrodes on separate sides of an ion-selective membrane. The redox chemistry at the electrodes' surfaces results in a flow of electrons through an external circuit accompanied by ion transfer through the membrane. The chemical potentials of the chemical components determine the cell voltage. At the same time, the energy capacity depends on the electrolyte volume, and the power depends on the surface area of the electrodes.

Unlike a traditional battery, like a Li-ion battery, where storage and conversion both occur in one entity of the battery cell, the electrode, in an RFB, the converter and the container for the "fuel" are separated. This separation of energy and power has advantages regarding the design of such systems, e.g., doubling the capacity of the battery is possible by simply doubling the size of the tank. (Doubling the capacity of a Li-ion battery is much more costly and cumbersome.) In addition, unlike traditional batteries, in an RFB, only a few percent of the total stored energy is connected electrochemically at any one time, which limits the risk of a runaway or uncontrolled energy release. Because flow can easily be stopped during a fault condition, the vulnerability to runaway is significantly reduced. Still, RFBs have their limitations. For example, the most common type of redox flow battery, the vanadium-based RFB, is limited to a low energy density because the redox process only involves one electron per ion. In addition, it offers a low power density because of the slow rate constant of the process. Finally, vanadium-based RFBs use a highly corrosive and environmentally damaging liquid for operation.

Converting Problems to Advantages in Redox-flow Batteries Using Polyoxometalates (POMs)

Chemical Characteristics

It is highly desirable to have an energy and power capability similar to Li-ion batteries and the flexibility of an RFB concept but with safe and environmentally benign materials and processes. A possibility to achieve this is to use polyoxometalates (POMs) as redox systems in an aqueous solution close to neutral pH. POMs are complex ions with multiple redox centers of the same or different metals. For example, SiW_{12}, which has the formula of $[SiW_{12}O_{40}]^{4-}$, is an approximately spherical cluster of tungsten atoms bound to oxygen and a central silicon atom (**Figure 1**). Similarly, PV_{14} (**Figure 2**), which has the formula $[PV_{14}O_{42}]^{9-}$, is a cluster of vanadium atoms bound to oxygen and a central phosphorus atom. In an RFB, POMs offer several advantages over dissolved metals like vanadium: (1) POMs can deliver multiple electrons, (2) POMs offer relatively high solubilities (often >0.5 M), which enables higher energy content; (3) POMs are typically very stable, capable of withstanding more than 20,000 charge-discharge cycles without significant degradation; (4) Because POMs have delocalized electron density, electron transfer is very fast (e.g., for PV_{14}, it is 10^4 times faster than for the V ion itself); and (5) POMs are made of environmentally benign and inexpensive materials.

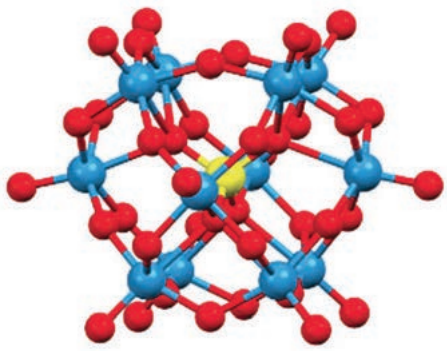

Figure 1. Model of SiW_{12}.

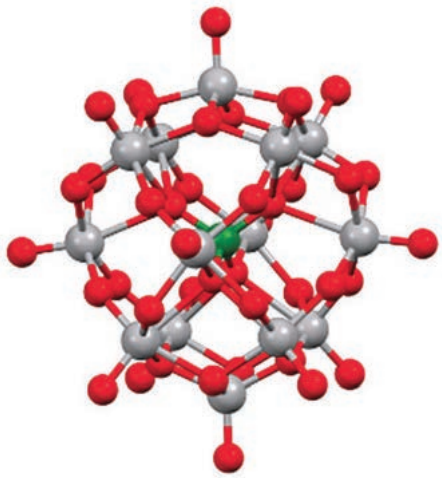

Figure 2. Model of PV_{14}.

An RFB battery based on POMs offers high energy density and high-power density at the same time. Coupled with the advantages of inexpensive and environmentally benign materials, POM-based RFBs have applications in three fields: mobility, power grid, and decentralized storage.

Mobility

Mobility is currently a hot topic regarding electrification. For automobile battery solutions, Li-ion batteries are presently favored. There are various challenges with the technology, as already noted, but limited resources for materials, limited power capabilities, and missing infrastructure are the most severe ones. Some of these challenges are so severe that using lithium-ion batteries in electric trucks is questionable. With the one liquid POM-RFB, we can achieve energy densities at par with Li-ion, but power densities are up to 50% higher than with Li-ion.

Table 1. Energy and power densities of battery systems [Litricity, patent application to EPO]

POM system or battery	gravimetric energy density /kWh/kg	volumetric energy density /kWh/L	gravimetric power density /kW/kg	volumetric power density / kW/L
POM 1	0.21	0.43	0.38	0.75
POM 2	0.20	0.31	0.35	0.56
Tesla 85kWh battery	0.21	0.32	0.21	0.31

The following example illustrates the situation: If you take a Li-ion battery in a Tesla Model S vehicle of 85 kWh, the whole system has a volume and mass of 263 L and 400 kg, respectively. A one-liquid POM system of the same capacity has a volume of 200 l and a mass of 400 kg. The resulting specific values are 0.21 kWh/kg for both and 0.43 kWh/L (POM) and 0.32 kWh/L (Tesla). Considering the power capabilities, the comparison is 0.38 kW/kg and 0.75 kW/L (POM) and 0.21 kW/kg and 0.31 kW/L (Tesla), respectively (see Table 1). Considering even some variations in numbers, performance data are at par, with a somewhat better power density for the POM system.

However, the most striking advantage for RFBs in mobile energy storage applications is that the charging process consists of exchanging the spent solution with a fresh one, comparable to the current process of refueling your car with gasoline. This process is faster than the slow charging times for current LIB batteries. It could leverage the existing fuel storage and distribution infrastructure, in contrast to LIB battery technology, which requires new infrastructure and capital investment to create the infrastructure. The RFB concept also enables electric-powered trucks to avoid extra weight problems with scaled-up lithium-ion batteries and their long charging times.

Power Grid

RFBs can also find use in storing energy to stabilize the power grid. In most countries, power plant capacity is laid out to cover all peak loads that can occur in the electric grid. The most common ones are the typical morning and evening peaks. Providing extra electricity during peak times requires large amounts of electricity and fast response. The state-of-the-art vanadium-based RFBs are too slow to respond to the changes in the grid, but POM-based RFBs have power capabilities about 104 times larger than vanadium-based RFBs. This allows for large electricity transfers in the sub-ms regime, a necessity for a fast frequency stabilization of the electric grid. A rough estimate shows that, e.g., in Germany, 20 to 30% of the power plants could be shut down due to this enormous load leveling effect. Beneficial for the environment, this could be a shutdown of most coal-fired power plants. In addition, such storage power stations provide grid stability by integrating renewable energy resources. Due to the extremely low self-discharge rates, it can provide a constant supply to the grid from unstable sources like solar or wind power over days or weeks.

Decentralized Storage

RFBs may provide a solution to decentralized energy storage as well, energy off grids. In an area of increased importance, the local building-related energy storage based on PV and/or small wind turbines, this concept can be beneficial. An RFB is comparable in performance to Li-ion batteries and is much safer because the risk of uncontrolled energy release is significantly reduced. In addition, RFBs may offer longer lifetimes and lower costs.

Conclusions

We advanced to an essential level in the current search for the holy grail of electricity storage. While validation is still needed, the POM-based battery systems tick the boxes of many aspects important for electricity storage, like capacity, power, ease of operation and transport, durability, sustainability, and, eventually, low cost of storing electricity. There may be better systems in the future. Still, this technology allows us to broadly introduce and use energy storage for many applications making fossil fuels more and more obsolete.

References

(1) Friedl, J.; Al-Oweini, R.; Herpich, M.; Keita, B.; Kortz, U.; Stimming, U. *Electrochim. Acta* **2014**, *141*, 357. DOI:10.1002/celc.201701246

(2) Al-Oweini, R.; Bassil, B.; Friedl, J.; Kottisch, V.; Ibrahim, M.; Asano, M.; Keita, B.; Novitchi, G.; Lan, Y.; Powell, A.; et. al. *Inorg. Chem.* **2014**, *53*, 5663. DOI:h10.1021/ic500425c

(3) Haider, A.; Ibrahim, M.; Bassil, B. S.; Carey, A. M.; Viet, A. N.; Xing, X.; Ayass, W. W.; Minambres, J. F.; Liu, R.; Zhang, G.; et. al. *Inorg. Chem.* **2016**, *55*, 2755. DOI:10.1021/acs.inorgchem.5b02503

(4) Chen, H-Y.; Friedl, J.; Pan, C-J.; Haider, A.; Al-Oweini, R.; Cheah, Y. L.; Lin, M-H.; Kortz, U.; Hwang, B-J.; Srinivasan, M.; Stimming, U. *Phys. Chem. Chem. Phys.* **2017**, *19*, 3358. DOI:10.1039/C6CP05768C

(5) Friedl, J.; Holland-Cunz, M. V.; Cording, F.; Panschilling, F. L.; Wills, C.; McFarlane, W.; Schricker, B.; Fleck, R.; Wolfschmidt, H.; Stimming, U. *Energy Environ. Sci.* **2018**, *11*, 3010. DOI:10.1039/C8EE00422F

(6) Holland-Cunz, M. V.; Cording, F.; Friedl, J.; Stimming, U. *Front. Energy* **2018**, *12*, 198. DOI:10.1007/s11708-018-0552-4

(7) Friedl, J.; Pfanschilling, F. L.; Holland-Cunz, M. V.; Fleck, R.; Schricker, B.; Wolfschmidt, H.; Stimming, U. *Clean Energy* **2019**, *3*, 278. DOI:10.1093/ce/zkz019

(8) Litricity – liquid electricity - https://litricity.de/

Solid Oxide Fuel Cells (SOFCs)

Name	Form	Purity	Cat. No.
Tris(cyclopentadienyl)yttrium(III)	solid	99.9% trace metals basis	**491969-1G**
Zirconium(IV) oxide-yttria stabilized	nanopowder	92% ZrO_2 basis	**572349-25G**
Tetrakis(dimethylamido)zirconium(IV)	solid	≥99.99% trace metals basis	**579211-5G**
Zirconium(IV) oxide-yttria stabilized	solid	99.9% trace metals basis	**774049-1EA**
Zirconium yttrium alloy	solid	99.9% trace metals basis (excluding ≤1% Hf)	**774057-1EA**

Fuel-Cell Membranes

Proton-Exchange Membranes

Name	L x W (cm)	Thickness (µm)	Cat. No.
Xion PEM-Aquivion®-720	5 x 5	5	**PEM3A0522-1EA**
	5 x 5	10	**PEM3A1022-1EA**
	5 x 5	20	**PEM3A2022-1EA**
	5 x 5	30	**PEM3A3022-1EA**
	5 x 5	50	**PEM3A5022-1EA**
	10 x 10	5	**PEM3A0544-1EA**
	10 x 10	10	**PEM3A1044-1EA**
	10 x 10	20	**PEM3A2044-1EA**
	10 x 10	30	**PEM3A3044-1EA**
	10 x 10	50	**PEM3A5044-1EA**
	15 x 15	5	**PEM3A0566-1EA**
	15 x 15	10	**PEM3A1066-1EA**
	15 x 15	20	**PEM3A2066-1EA**
	15 x 15	30	**PEM3A3066-1EA**
	15 x 15	50	**PEM3A5066-1EA**
Xion PEM-Aquivion®-830	5 x 5	5	**PEM3B0522-1EA**
	5 x 5	10	**PEM3B1022-1EA**
	5 x 5	20	**PEM3B2022-1EA**
	5 x 5	30	**PEM3B3022-1EA**
	5 x 5	50	**PEM3B5022-1EA**
	10 x 10	5	**PEM3B0544-1EA**
	10 x 10	10	**PEM3B1044-1EA**
	10 x 10	20	**PEM3B2044-1EA**
	10 x 10	30	**PEM3B3044-1EA**
	10 x 10	50	**PEM3B5044-1EA**
	15 x 15	5	**PEM3B0566-1EA**
	15 x 15	10	**PEM3B1066-1EA**
	15 x 15	20	**PEM3B2066-1EA**
	15 x 15	30	**PEM3B3066-1EA**
	15 x 15	50	**PEM3B5066-1EA**
Xion PEM-Dyneon-725	5 x 5	5	**PEM1A0522-1EA**
	5 x 5	10	**PEM1A1022-1EA**
	5 x 5	20	**PEM1A2022-1EA**
	5 x 5	30	**PEM1A3022-1EA**
	5 x 5	50	**PEM1A5022-1EA**
	10 x 10	5	**PEM1A0544-1EA**
	10 x 10	10	**PEM1A1044-1EA**
	10 x 10	20	**PEM1A2044-1EA**
	10 x 10	30	**PEM1A3044-1EA**
	10 x 10	50	**PEM1A5044-1EA**
	15 x 15	5	**PEM1A0566-1EA**
	15 x 15	10	**PEM1A1066-1EA**
	15 x 15	20	**PEM1A2066-1EA**
	15 x 15	30	**PEM1A3066-1EA**
	15 x 15	50	**PEM1A5066-1EA**

Name	L x W (cm)	Thickness (µm)	Cat. No.
Xion PEM-Dyneon-800	5 x 5	5	**PEM1B0522-1EA**
	5 x 5	10	**PEM1B1022-1EA**
	5 x 5	20	**PEM1B2022-1EA**
	5 x 5	30	**PEM1B3022-1EA**
	5 x 5	50	**PEM1B5022-1EA**
	10 x 10	5	**PEM1B0544-1EA**
	10 x 10	10	**PEM1B1044-1EA**
	10 x 10	20	**PEM1B2044-1EA**
	10 x 10	30	**PEM1B3044-1EA**
	10 x 10	50	**PEM1B5044-1EA**
	15 x 15	5	**PEM1B0566-1EA**
	15 x 15	10	**PEM1B1066-1EA**
	15 x 15	20	**PEM1B2066-1EA**
	15 x 15	30	**PEM1B3066-1EA**
	15 x 15	50	**PEM1B5066-1EA**
Xion PEM-Nafion™-1000	5 x 5	5	**PEM2A0522-1EA**
	5 x 5	10	**PEM2A1022-1EA**
	5 x 5	20	**PEM2A2022-1EA**
	5 x 5	30	**PEM2A3022-1EA**
	5 x 5	50	**PEM2A5022-1EA**
	10 x 10	5	**PEM2A0544-1EA**
	10 x 10	10	**PEM2A1044-1EA**
	10 x 10	20	**PEM2A2044-1EA**
	10 x 10	30	**PEM2A3044-1EA**
	10 x 10	50	**PEM2A5044-1EA**
	15 x 15	5	**PEM2A0566-1EA**
	15 x 15	10	**PEM2A1066-1EA**
	15 x 15	20	**PEM2A2066-1EA**
	15 x 15	30	**PEM2A3066-1EA**
	15 x 15	50	**PEM2A5066-1EA**
Xion PEM-Nafion™-1100	5 x 5	5	**PEM2B0522-1EA**
	5 x 5	10	**PEM2B1022-1EA**
	5 x 5	20	**PEM2B2022-1EA**
	5 x 5	30	**PEM2B3022-1EA**
	5 x 5	50	**PEM2B5022-1EA**
	10 x 10	5	**PEM2B0544-1EA**
	10 x 10	10	**PEM2B1044-1EA**
	10 x 10	20	**PEM2B2044-1EA**
	10 x 10	30	**PEM2B3044-1EA**
	10 x 10	50	**PEM2B5044-1EA**
	15 x 15	5	**PEM2B0566-1EA**
	15 x 15	10	**PEM2B1066-1EA**
	15 x 15	20	**PEM2B2066-1EA**
	15 x 15	30	**PEM2B3066-1EA**
	15 x 15	50	**PEM2B5066-1EA**

Anion-Exchange Membranes

Name	L x W (cm)	Thickness (µm)	Cat. No.
Xion AEM-Pention-72-5CL	5 x 5	5	**AEM2A0522-1EA**
	5 x 5	10	**AEM2A1022-1EA**
	5 x 5	20	**AEM2A2022-1EA**
	5 x 5	30	**AEM2A3022-1EA**
	5 x 5	50	**AEM2A5022-1EA**
	10 x 10	5	**AEM2A0544-1EA**
	10 x 10	10	**AEM2A1044-1EA**
	10 x 10	20	**AEM2A2044-1EA**
	10 x 10	30	**AEM2A3044-1EA**
	10 x 10	50	**AEM2A5044-1EA**
	15 x 15	5	**AEM2A0566-1EA**
	15 x 15	10	**AEM2A1066-1EA**
	15 x 15	20	**AEM2A2066-1EA**
	15 x 15	30	**AEM2A3066-1EA**
	15 x 15	50	**AEM2A5066-1EA**
Xion AEM-Pention-72-15CL	5 x 5	5	**AEM2B0522-1EA**
	5 x 5	10	**AEM2B1022-1EA**
	5 x 5	20	**AEM2B2022-1EA**
	5 x 5	30	**AEM2B3022-1EA**
	5 x 5	50	**AEM2B5022-1EA**
	10 x 10	5	**AEM2B0544-1EA**
	10 x 10	10	**AEM2B1044-1EA**
	10 x 10	20	**AEM2B2044-1EA**
	10 x 10	30	**AEM2B3044-1EA**
	10 x 10	50	**AEM2B5044-1EA**
	15 x 15	5	**AEM2B0566-1EA**
	15 x 15	10	**AEM2B1066-1EA**
	15 x 15	20	**AEM2B2066-1EA**
	15 x 15	30	**AEM2B3066-1EA**
	15 x 15	50	**AEM2B5066-1EA**

Name	L x W (cm)	Thickness (µm)	Cat. No.
Xion AEM-Durion II-LMW	5 x 5	5	**AEM1A0522-1EA**
	5 x 5	10	**AEM1A1022-1EA**
	5 x 5	20	**AEM1A2022-1EA**
	5 x 5	30	**AEM1A3022-1EA**
	10 x 10	5	**AEM1A0544-1EA**
	10 x 10	10	**AEM1A1044-1EA**
	10 x 10	20	**AEM1A2044-1EA**
	10 x 10	30	**AEM1A3044-1EA**
	15 x 15	5	**AEM1A0566-1EA**
	15 x 15	10	**AEM1A1066-1EA**
	15 x 15	20	**AEM1A2066-1EA**
	15 x 15	30	**AEM1A3066-1EA**

Water-Exchange Membranes

Name	L x W (cm)	Thickness (µm)	Cat. No.
Xion WEM-Hydrex-200	5 x 5	30	**WEM1A3022-1EA**
	5 x 5	50	**WEM1A5022-1EA**
	10 x 10	30	**WEM1A3044-1EA**
	10 x 10	50	**WEM1A5044-1EA**
	15 x 15	30	**WEM1A3066-1EA**
	15 x 15	50	**WEM1A5066-1EA**

Product Highlight

Make Your Own Lithium-Ion Batteries

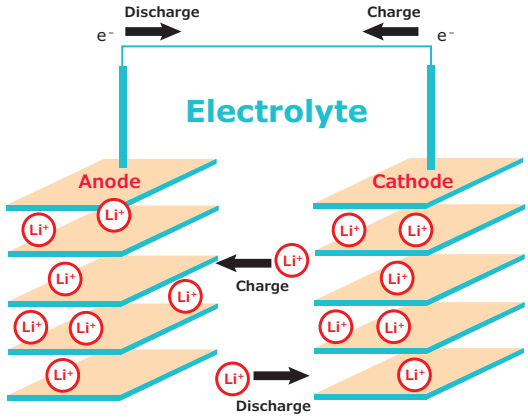

Applications of lithium-ion batteries (LIBs) extend from modern electronics to automobiles. Order ready-to-use electrolyte solutions and electrode sheets in battery grade to fabricate your LIB.

Electrolyte Solutions

H_2O < 15 ppm, HF < 50 ppm, APHA < 50

Name	Specifications	Cat. No.
2.0 M LiPF6 in EC/DMC=50/50 (v/v)	in ethylene carbonate and dimethyl carbonate	**809357**
2.0 M LiPF6 in EC/EMC=50/50 (v/v)	in ethylene carbonate and ethyl methyl carbonate	**809365**
2.0 M LiPF6 in EC/DEC=50/50 (v/v)	in ethylene carbonate and diethyl carbonate	**809349**
2.0 M LiPF6 in DMC	in dimethyl carbonate	**809411**
2.0 M LiPF6 in EMC	in ethyl methyl carbonate	**809403**
2.0 M LiPF6 in DEC	in diethyl carbonate	**809543**
2.0 M LiPF6 in PC	in propylene carbonate	**809470**

Electrode Sheets

Aluminum substrate, size 5 in. × 10 in.

Name	Specifications	Composition	Cat. No.
Lithium nickel manganese cobalt oxide	loading >80%, thickness 25–50 µm	$LiNi_{0.33}Mn_{0.33}Co_{0.33}O_2$	**765163**
Lithium nickel cobalt aluminum oxide	loading >80%, thickness 12–25 µm	$LiNi_{0.8}Co_{0.15}Al_{0.05}O_2$	**765171**
Lithium manganese nickel oxide	loading >80%, thickness 25–50 µm	$Li_2Mn_3NiO_8$	**765198**
Lithium manganese oxide	loading >80%, thickness 25–40 µm	$LiMn_2O_4$	**765201**
Lithium titanate spinel	loading >80%, thickness 25–50 µm	$Li_4Ti_5O_{12}$	**765155**

To find out more, visit
SigmaAldrich.com/LIB

Merck KGaA
Frankfurter Strasse 250
64293 Darmstadt, Germany

Silicon Anode Materials

for High-capacity Cathode Research

With a capacity over 1300 mAh/g, our silicon composite formulation is well suited for use as a counter electrode for new high capacity cathode materials.

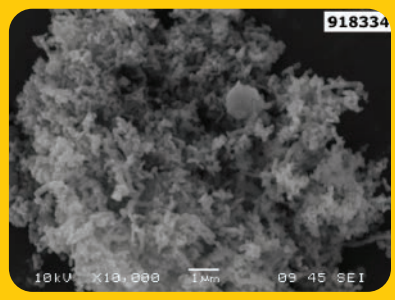

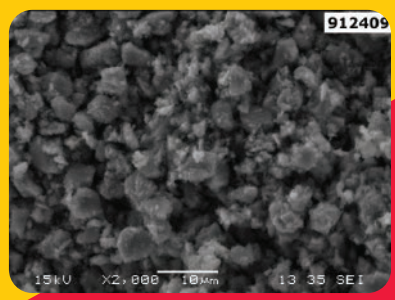

Test your batteries longer with our silicon composite anodes. Unlike some silicon-based electrode formulations, our 3D porous conductive polymer prevents capacity loss during the charge/ discharge cycles.

SigmaAldrich.com/si-anode

The Life Science business of Merck operates as MilliporeSigma in the U.S. and Canada.

MK_BR11901EN 12/2022

Sigma-Aldrich®
Lab & Production Materials